RECOIL POLARIZATION FOR NEUTRAL PION ELECTROPRODUCTION NEAR THE DELTA RESONANCE

JAMES J. KELLY
for the Jefferson Laboratory Hall A Collaboration

Department of Physics, University of Maryland, College Park, MD 20742

We have measured angular distributions for recoil polarization in the $p(\vec{e},e'\vec{p})\pi^0$ reaction at $Q^2 \approx 1$ (GeV/c)^2 with $1.16 \leq W \leq 1.36$ GeV across the Δ resonance. The data are compared with representative models and a truncated Legendre analysis is compared with a more general multipole analysis.

PACS numbers: 13.60.Le, 13.88.+e, 14.20.Gk
Keywords: pion electroproduction, recoil polarization, delta resonance, multipole analysis

I. INTRODUCTION

Transition form factors for the electroexcitation of nucleon resonances provide stimulating tests of QCD-inspired models of baryon structure. For the Δ resonance, in particular, there has been long-standing interest in deformed components of the N and Δ wave functions. The dominant amplitude for pion electroproduction at the Δ resonance is the M_{1+} amplitude, but smaller S_{1+} and E_{1+} amplitudes arise from configuration mixing within the quark core [1], often described as quadrupole deformation, or from meson and gluon exchange currents between quarks [2], or coupling to the pion cloud outside the quark core [3, 4]. Thus, the quadrupole deformation is related to the ratios of isospin-3/2 electroproduction multipole amplitudes EMR = Re($E_{1+}^{3/2}/M_{1+}^{3/2}$) and SMR = Re($S_{1+}^{3/2}/M_{1+}^{3/2}$) evaluated at $W = M_\Delta$ where $M_\Delta = 1.232$ GeV is the physical mass. It has been argued that the intrinsic N and Δ quadrupole moments are small [5] and that the observed EMR and SMR are dominated by nonvalence degrees of freedom. However, extraction of these amplitudes from the differential cross section for pion electroproduction is also quite model dependent and requires understanding backgrounds from nonresonant production mechanisms and underlying tails of nondominant resonances. This model dependence can be reduced considerably by measurement of recoil and/or target polarization observables that are sensitive to the relative phase between resonant and nonresonant mechanisms. Then it may be possible to perform a nearly model-independent multipole analysis if a sufficiently large number of observables become available with some sensitive to real parts and others to imaginary parts of products of multipole amplitudes.

We have measured recoil polarization in the $p(\vec{e},e'\vec{p})\pi^0$ reaction at $Q^2 \approx 1$ (GeV/c)^2 near the Δ resonance, obtaining angular distributions for a total of 16 independent response functions in a 5×2 grid of (W, Q^2). We compare a traditional truncated Legendre analysis with a more general multipole analysis of these data. Section II defines the response functions, Sec. III describes the experiment, Sec. IV compares the data with selected models and compares Legendre and multipole analyses, and Sec. V summarizes our conclusions.

II. RESPONSE FUNCTIONS

The differential cross section for recoil polarization in the pion electroproduction reaction $p(\vec{e}, e'\vec{N})\pi$ can be expressed in the form

$$\frac{d^5\sigma}{dk_f d\Omega_e d\Omega^*} = \Gamma_\gamma \bar{\sigma} \left[1 + hA + \mathbf{\Pi} \cdot \boldsymbol{S}\right] \tag{1}$$

where $\bar{\sigma}$ is the unpolarized cross section, h is the electron helicity, $\boldsymbol{S}$ is the spin direction for the recoil nucleon, A is the beam analyzing power, $\mathbf{\Pi} = \boldsymbol{P} + h\boldsymbol{P'}$ is the recoil polarization,

$$\Gamma_\gamma = \frac{\alpha}{2\pi^2} \frac{k_f}{k_i} \frac{k_\gamma}{Q^2} \frac{1}{1-\epsilon} \tag{2}$$

is the virtual photon flux for initial (final) electron momenta k_i (k_f), $\epsilon = \left(1 + 2\frac{\mathbf{q}^2}{Q^2} \tan^2 \frac{\theta_e}{2}\right)^{-1}$ is the transverse polarization of the virtual photon, θ_e is the electron scattering angle, and $k_\gamma = (W^2 - m_p^2)/2m_p$ is the laboratory energy a real photon would need to excite the same transition. Note that electron kinematics and solid angle $d\Omega_e$ are normally expressed in the lab frame while hadron kinematics and nucleon solid angle $d\Omega^*$ are expressed in the πN cm frame.

It is convenient to express polarization vectors in a basis where $\hat{\ell}$ is along the nucleon momentum in the cm frame, $\hat{n} \propto \hat{q} \wedge \hat{\ell}$ is normal to the reaction plane, and $\hat{t} = \hat{n} \wedge \hat{\ell}$. The azimuthal dependence can then be extracted and the observables can be decomposed into kinematical factors, ν_α, which depend only upon electron kinematics and response functions, $R_\alpha(x, W, Q^2)$, which carry the hadronic information, such that

$$\begin{aligned}
\bar{\sigma} &= \nu_0 \left[\nu_L R_L + \nu_T R_T + \nu_{LT} R_{LT} \cos\phi + \nu_{TT} R_{TT} \cos 2\phi\right] && \text{(3a)}\\
A\bar{\sigma} &= \nu_0 \left[\nu'_{LT} R'_{LT} \sin\phi\right] && \text{(3b)}\\
P_n\bar{\sigma} &= \nu_0 \left[\nu_L R^n_L + \nu_T R^n_T + \nu_{LT} R^n_{LT} \cos\phi + \nu_{TT} R^n_{TT} \cos 2\phi\right] && \text{(3c)}\\
P_{\ell,t}\bar{\sigma} &= \nu_0 \left[\nu_{LT} R^{\ell,t}_{LT} \sin\phi + \nu_{TT} R^{\ell,t}_{TT} \sin 2\phi\right] && \text{(3d)}\\
P'_n\bar{\sigma} &= \nu_0 \left[\nu'_{LT} R'^n_{LT} \sin\phi\right] && \text{(3e)}\\
P'_{\ell,t}\bar{\sigma} &= \nu_0 \left[\nu'_{LT} R'^{\ell,t}_{LT} \cos\phi + \nu'_{TT} R'^{\ell,t}_{TT}\right] && \text{(3f)}
\end{aligned}$$

where the response functions depend upon W, Q^2, and $x = \cos\theta_\pi$ where θ_π is the pion angle relative to $\vec{q}$ in the πN center of mass frame. The phase-space factor $\nu_0 = k/q_0$ is usually taken as the ratio between the cm momentum in the final state and the cm momentum a real photon needs for the same transition. The remaining kinematical coefficients are given by: $\nu_T = 1$, $\nu_{TT} = \epsilon$, $\nu'_{TT} = \sqrt{1-\epsilon^2}$, $\nu_L = \epsilon_S$, $\nu_{LT} = \sqrt{2\epsilon_S(1+\epsilon)}$, and $\nu'_{LT} = \sqrt{2\epsilon_S(1-\epsilon)}$ where $\epsilon_S = \frac{Q^2}{q^2}\epsilon$. When there is insufficient information to perform a Rosenbluth separation, we employ ϵ-dependent combinations

$$\begin{aligned}
\nu_T R_{L+T} &= \nu_L R_L + \nu_T R_T && \text{(4a)}\\
\nu_T R^n_{L+T} &= \nu_L R^n_L + \nu_T R^n_T && \text{(4b)}
\end{aligned}$$

III. EXPERIMENT

The experiment was performed in Hall A of Jefferson Laboratory using a 4.531 GeV electron beam with an average current of 45 μA for 36.5 days and longitudinal polarization varying between 57 and 75% incident upon a 15 cm LH_2 target. The polarization was monitored nearly continuously by a Compton polarimeter. In addition, a few measurements were also made with a Moller polarimeter. Scattered electrons and protons were detected in a pair of nearly identical high resolution spectrometers with nominal acceptances of $\Delta\Omega = 6$ msr and $\Delta p/p = \pm 4.5\%$. The electron spectrometer remained fixed at $\theta_e = 14.1^\circ$ with a central momentum of 3.66 GeV/c for central values $(W, Q^2) = (1.232$ GeV, 1.0 $(\mathrm{GeV}/c)^2)$ with $\epsilon \approx 0.95$. Twelve settings of the proton spectrometer covered the angular distribution for pion electroproduction. Although the spectrometers are confined to the horizontal plane, the kinematic focussing into a reaction cone with opening angle of approximately 13° provides considerable out-of-plane coverage, especially for $x \sim -1$.

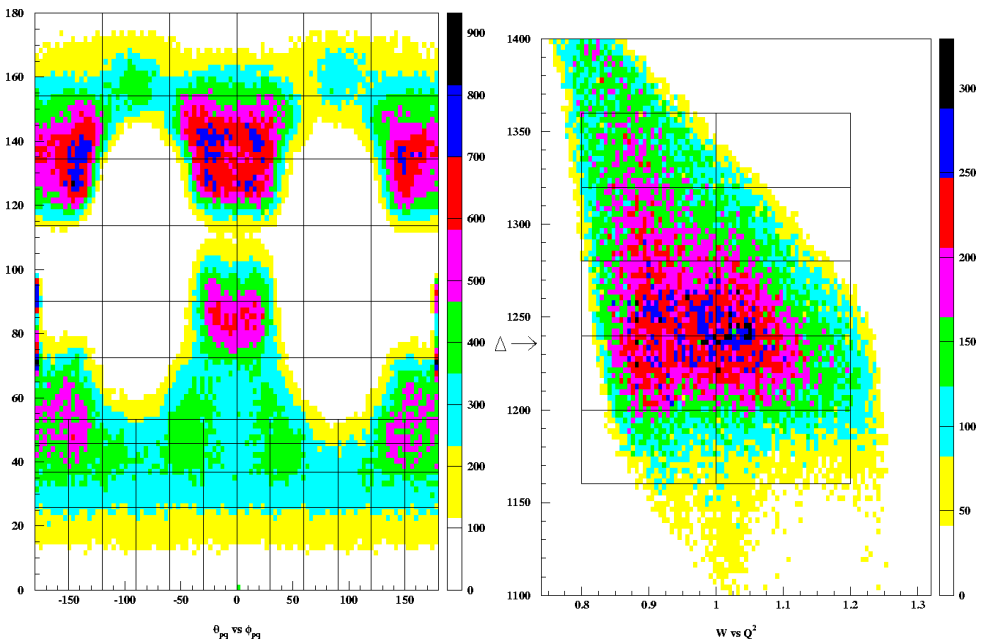

FIG. 1: Kinematical acceptance and the binning for the polarization analysis. Left: angular acceptance for θ_N, ϕ_N in the cm frame. Right: (W, Q^2) acceptance.

The proton polarization was measured using a focal-plane polarimeter (FPP) with a carbon analyzer; the carbon thickness was adjusted to obtain optimal figure-of-merit for each proton momentum setting. Response functions and polarization at the target were extracted from the azimuthal distribution using the method of maximum likelihood. Good agreement was obtained with previous measurements for proton elastic scattering [6]. Helicity-independent asymmetries for elastic scattering were used to parametrize instrumental asymmetries, which were generally less than 1%. Angular distributions for 14 separated response functions and 2 Rosenbluth combinations were obtained in the 5×2 grid of (W, Q^2) indicated in Fig. 1, although the statistics in the lower-left and upper-right corners were quite limited. Details of the analysis can be found in Refs. [7, 8].

IV. RESULTS

Preliminary data for $(W, Q^2) = (1.22 \pm 0.02, 0.9 \pm 0.1)$ are shown in Fig. 2. The unpolarized response functions are compared with the published Hall B data of Joo *et al.* [9]. Note that the Hall B data for R_{L+T} contain two beam energies while the Hall A data for $\epsilon \sim 0.95$ lie slightly higher, as expected. In general we find good agreement between the two experiments, but the statistical precision of the present data is considerably higher than that of the published Hall B data; higher statistics from the latter will be forthcoming. The limited spectrometer acceptance in ϕ for $x \sim 0$ does not permit separation there between R_{L+T} and R_{TT}, but the cross section data (not shown) were included in the partial-wave and multipole analyses.

The 12 response functions shown in columns 2–4 of Fig. 2 have been observed here for the first time. The response functions in the third column depend upon real parts of interference products and are dominated by resonant amplitudes while those in the second and fourth columns depend upon imaginary parts and are more sensitive to the nonresonant contributions. Consequently, model differences are more pronounced for the latter. The data are compared with calculations based upon the MAID2000 [10], DMT [11], and SAID [12] models. Of these, the DMT model gives the best overall qualitative agreement with the data, but none are really satisfactory.

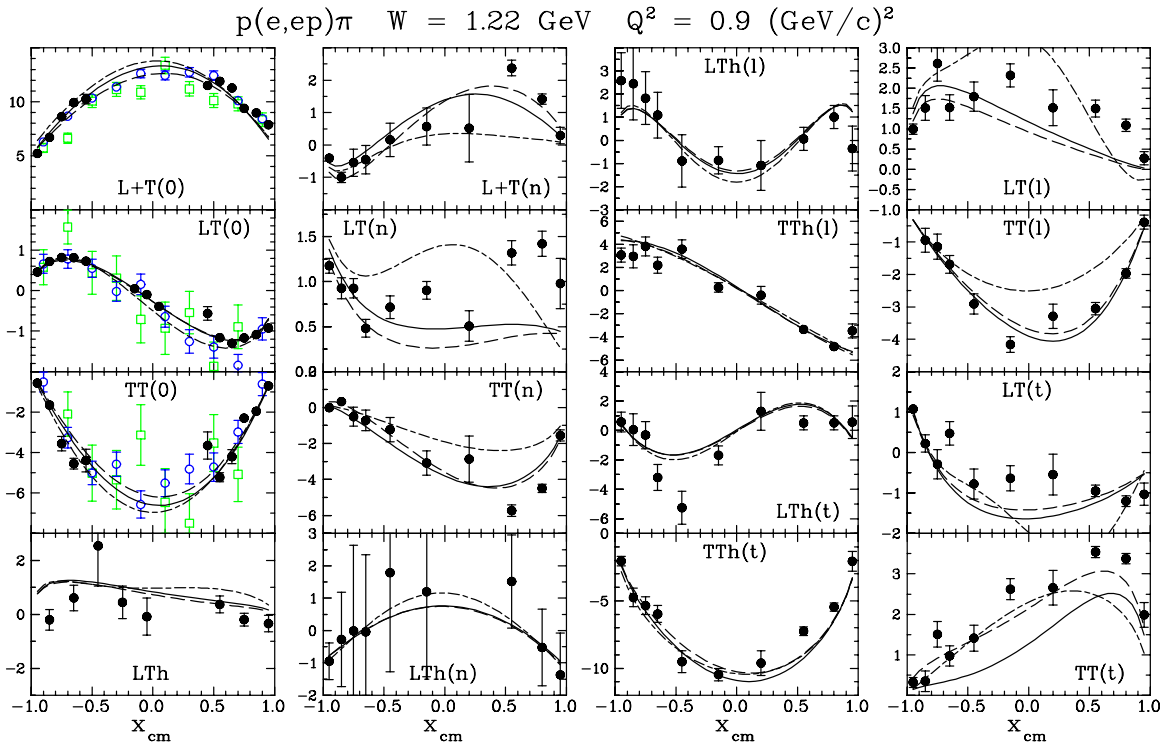

FIG. 2: Data for response functions at $(W, Q^2) = (1.22, 0.9)$ are compared with selected models: MAID2000 (solid), DMT (dashed), SAID (dash-dot). Results from CLAS are shown as green squares for $k_i = 1.645$ GeV or blue open circles for $k_i = 2.445$ GeV. For each panel, the first part of the label describes the interference structure, inclusion of "h" indicates helicity dependence, and the recoil polarization is given in parentheses with "0" indicating an unpolarized response.

A. Legendre Analysis

Each of the response functions can be represented by a Legendre expansion of the form

$$R_\eta = (1-x^2)^{\alpha_\eta/2} \sum_{n=0}^{\infty} A_n^\eta P_n(x) \tag{5}$$

where α_η represents the leading angular dependence for the response function identified by η. Clearly, response functions with $\alpha_\eta > 0$ vanish for parallel or antiparallel kinematics where $x^2 = 1$. The Legendre coefficients $A_n^\eta(W, Q^2)$ can be obtained by fitting response-function angular distributions for each (W, Q^2). Alternatively, often the most efficient method for extracting the x dependence of response functions for a particular (W, Q^2) bin is to perform a two-dimensional fit of the (x, ϕ) dependencies of the appropriate observable, cross section or polarization, with the aid of the Legendre expansion. This type of analysis can be used to extrapolate response functions to parallel or antiparallel kinematics where interesting symmetry relations have been developed but where the experimental acceptance vanishes.

The Legendre coefficients can be expanded in terms of products of multipole amplitudes, but unwieldy general expressions are omitted. Most analyses in the Δ region have limited the expansions to s- and p-waves and have used the assumption of M_{1+} dominance to truncate these expansions to terms involving the M_{1+} amplitude. Thus, using the coefficients fitted to the unpolarized cross sections one would deduce

$$\frac{\mathrm{Re}E_{1+}^* M_{1+}}{|M_{1+}|^2} \approx \frac{3A_2^{L+T} - 2A_0^{TT}}{12A_0^{L+T}} \tag{6a}$$

$$\frac{\mathrm{Re}S_{1+}^* M_{1+}}{|M_{1+}|^2} \approx \frac{A_1^{LT}}{3A_0^{L+T}} \tag{6b}$$

However, similar expressions can be obtained from truncated multipole expansions of the Legendre coefficients for other response functions also and there is no guarantee of consistency between these determinations because the Legendre analysis treats each response function independently without regard to its multipole content. Furthermore, Legendre fits limited to the number of terms suggested by M_{1+} dominance fail to reproduce some of the response functions, demonstrating that higher-order terms are not always negligible. The dashed lines in Fig. 3 show that M_{1+} dominance is sufficient to fit most of the response functions well, but several response functions require additional terms. The solid curves include one or two additional terms for response functions that are not described well by the *sp* trunction over a range of (W, Q^2). CLAS data were not included in the fits.

B. Multipole Analysis

Our nearly complete set of recoil-polarization response functions make it possible to perform a more rigorous multipole analysis. Let

$$A_i(W, Q^2) = A_i^{(0)}(W, Q^2) + \delta A_i(W, Q^2) \tag{7}$$

represent either the real or the imaginary part of one of the multipole amplitudes ($M_{\ell j}$, $E_{\ell j}$, or $S_{\ell j}$) where $A_i^{(0)}$ is a baseline amplitude obtained from a suitable model, usually

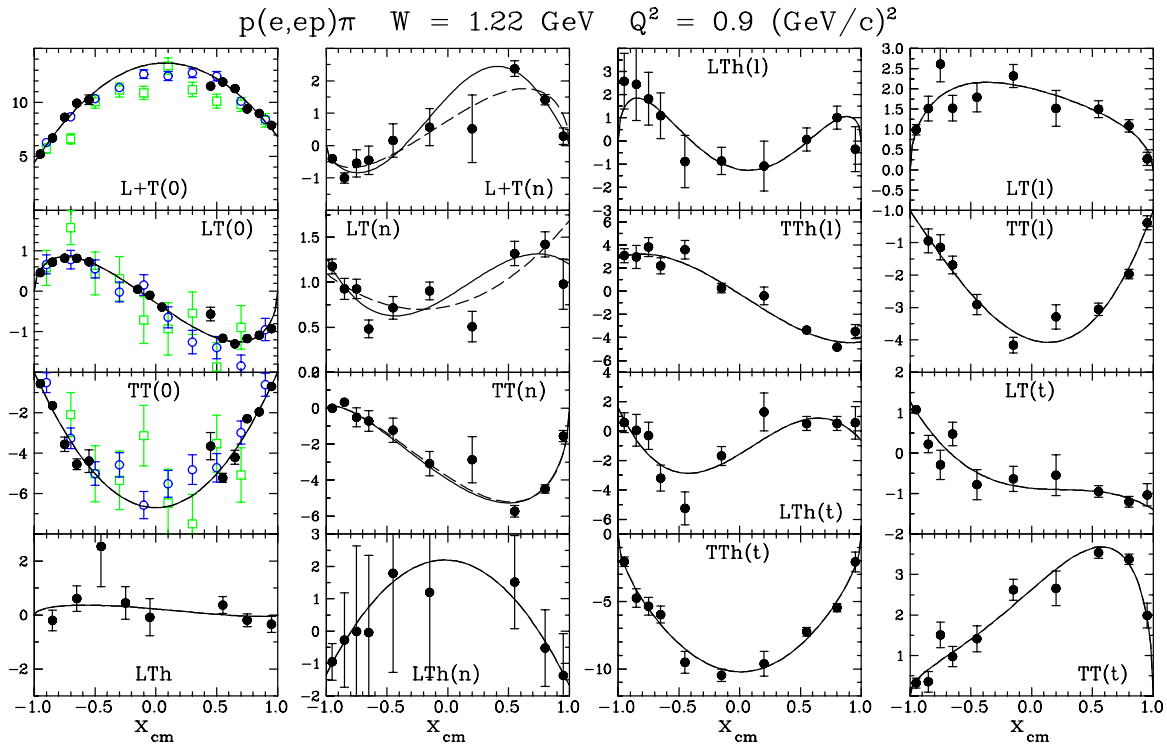

FIG. 3: Data for response functions at $(W, Q^2) = (1.22, 0.9)$ are compared with Legendre fits in the *sp* truncation (dashed) and with a few extra terms as needed (solid). Results from CLAS are shown as green squares for $k_i = 1.645$ GeV or blue open circles for $k_i = 2.445$ GeV.

MAID or DMT, while δA_i is a variable to be fit to the data. If we were to limit the fit to variations of the s- and p-wave amplitudes, with all higher amplitudes determined by the selected baseline model, there would be up to 14 free parameters for each (W, Q^2) bin to be fit to the (x, ϕ) distributions for 8 measured quantities (cross section, analyzing power, and helicity-dependent and helicity-independent recoil polarization components) simultaneously. Alternatively, we can fit the parameters to the x distributions of the 16 response functions that are available without Rosenbluth separation. Variation of all d-wave amplitudes would increase the number of free parameters to 26 per (W, Q^2) bin while reducing the sensitivity to the choice of baseline model. In the Δ region one expects the higher multipoles to have relatively little influence and to be dominated by Born terms, which are similar in most models. The sensitivity of fitted multipole amplitudes to uncertainties in higher partial waves can be gauged by comparing fits using different baseline models. An advantage of this type of analysis is that it minimizes the dependence upon models; however, it does not guarantee that the fitted multipole amplitudes will depend smoothly on both W and Q^2. Model-dependent analyses which adjust parameters of an effective Lagrangian should produce kinematically smooth multipole amplitudes at the expense of possible bias.

The dashed lines in Fig. 4 show a fit that varies all s- and p-wave multipole amplitudes for $(W, Q^2) = (1.22, 0.9)$ while the solid lines vary d-wave amplitudes also. MAID2000 was used as the baseline model for higher partial waves. There appears to be no systematic improvement in the fits by varying d-wave amplitudes but the fits are not as accurate as the Legendre analysis either, which may indicate a deficiency of the nonresonant contributions to the baseline model or inconsistencies in the preliminary data. A revised analysis of the

response-function data that corrects some errors is in progress and final results are expected soon.

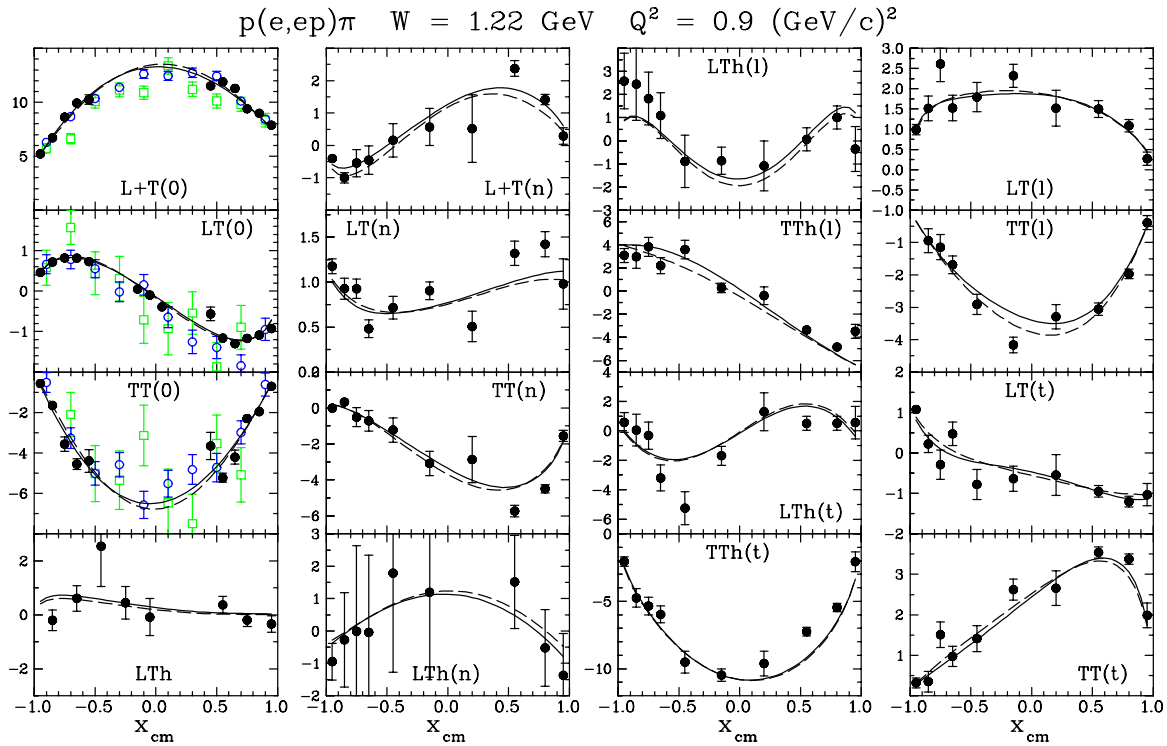

FIG. 4: Data for response functions at $(W, Q^2) = (1.22, 0.9)$ are compared with fits that vary *sp* (dashed) versus *spd* (solid) multipole amplitudes. Results from CLAS are shown as green squares for $k_i = 1.645$ GeV or blue open circles for $k_i = 2.445$ GeV.

The quadrupole deformation parameters can now be obtained directly from the fitted multipole amplitudes using

$$\frac{\mathrm{Re}E^*_{1+}M_{1+}}{|M_{1+}|^2} = \frac{\mathrm{Re}E_{1+}\mathrm{Re}M_{1+} + \mathrm{Im}E_{1+}\mathrm{Im}M_{1+}}{\mathrm{Re}M_{1+}\mathrm{Re}M_{1+} + \mathrm{Im}M_{1+}\mathrm{Im}M_{1+}} \tag{8a}$$

$$\frac{\mathrm{Re}S^*_{1+}M_{1+}}{|M_{1+}|^2} = \frac{\mathrm{Re}S_{1+}\mathrm{Re}M_{1+} + \mathrm{Im}S_{1+}\mathrm{Im}M_{1+}}{\mathrm{Re}M_{1+}\mathrm{Re}M_{1+} + \mathrm{Im}M_{1+}\mathrm{Im}M_{1+}} \tag{8b}$$

where $\mathrm{Re}M_{1+} \to 0$ at the physical mass, $W \to M_\Delta = 1.232$ GeV. The deformation of the $N \to \Delta$ transition is generally quoted at $W = 1.232$ GeV after correction for the isospin-1/2 contribution, but this correction has not yet been made. For fixed Q^2 we can interpolate within the W dependence of these ratios or employ a bin centered upon M_Δ.

These two methods for determination of EMR and SMR are compared in Fig. 5. The left panel uses Eq. (6) for the truncated Legendre analysis while the right panel uses Eq. (8) for the multipole analysis, where within each panel both data and calculations employ the same formulas. The difference between the two methods at $W = 1.232$ GeV is a measure of the accuracy of the truncated Legendre analysis. For the multipole analysis red points fit *s*- and *p*-wave multipoles with higher multipoles taken from MAID2000 while black points fit *d*-wave amplitudes also and have larger uncertainties because the data do not determine those amplitudes well enough. Note that the covariance matrix was used to evaluate the

effect of correlations upon the uncertainties in these ratios. The experimental results for SMR are stable and both methods give similar W dependencies over this entire range. The model calculations for SMR are also in agreement with the data near 1.232 GeV and describe the W dependencies well, although MAID2000 and DMT are in better agreement with each other than with SAID. For EMR, on the other hand, the two methods produce different W dependencies and the variation among models is greater; nevertheless, these variations remain fairly small in the immediate vicinity of M_Δ. The experimental results are more sensitive to the choice of variables and baseline model for EMR than for SMR.

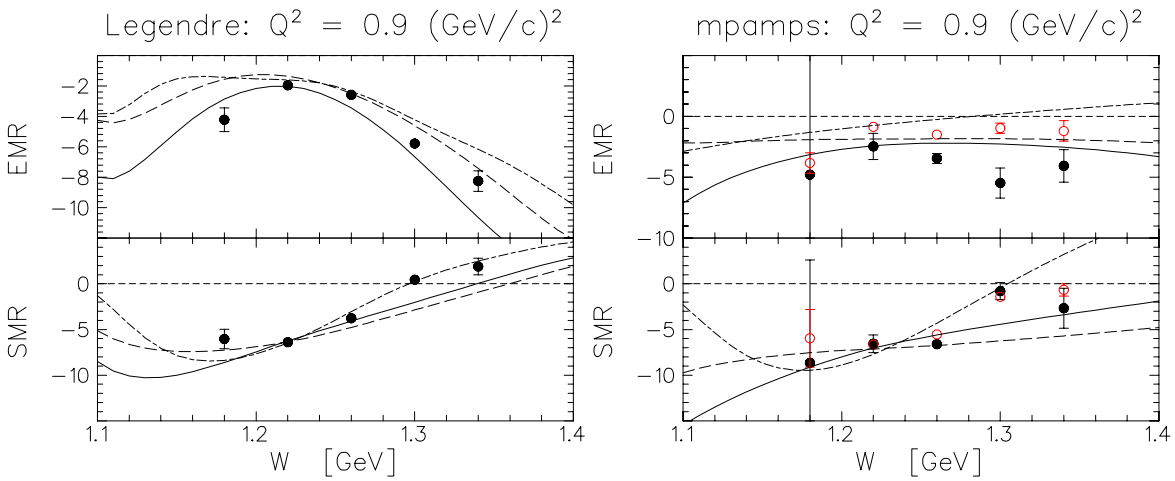

FIG. 5: EMR and SMR data for $Q^2 = 0.9$ (GeV/c)^2 are compared with MAID2000 (solid), DMT (dashed), and SAID (dash-dot). Left: results from truncated Legendre expansion. Right: results from multipole analysis with red points varying *sp* and black points varying *spd* amplitudes wrt MAID2000. Within each panel data and curves employ the same formulas.

The present analysis is still preliminary and should not be quoted before the remaining problems in the data analysis are resolved and a more detailed analysis of the model dependencies is made. These results should be regarded as an indication of what should be possible with the final data. A more detailed presentation of the multipole amplitudes will be made in a later publication.

V. SUMMARY

We have measured angular distributions for recoil polarization in the $p(\vec{e}, e'\vec{p})\pi^0$ reaction at $Q^2 \approx 1$ (GeV/c)^2 with $1.16 \leq W \leq 1.36$ GeV across the Δ resonance and have obtained 14 separated response functions and 2 Rosenbluth combinations, of which 12 have been measured for the first time. Calculations for quantities that depend upon real parts of interference products differ little among models and agree relatively well with the data, but variations among models and disagreements with data are much larger for quantities dependent upon imaginary parts that are more sensitive to background amplitudes. These data can be used to perform a multipole analysis in which the real and imaginary parts of multipoles for low partial waves are fit while higher nonresonant partial waves are constrained by models. This type of analysis is much more general than the truncated Legendre analysis normally used to determine EMR and SMR for the $N \rightarrow \Delta$ transition. For SMR we find

good agreement between these methods and relatively little model dependence, but results for EMR are more sensitive to the analysis method.

---

[1] N. Isgur, G. Karl, and R. Koniuk, Phys. Rev. **D 25**, 2394 (1982).

[2] U. Meyer, E. Hernández, and A. J. Buchmann, Phys. Rev. **C 64**, 035203 (2001).

[3] M. Fiolhais, G. Golli, and S. Sirca, Phys. Lett. **B373**, 229 (1996).

[4] S. S. Kamalov and S. N. Yang, Phys. Rev. Lett. **83**, 4494 (1999).

[5] A. J. Buchmann and E. M. Henley, Phys. Rev. **C 63**, 015202 (2000).

[6] M. K. Jones *et al.*, Phys. Rev. Lett. **84**, 1398 (2000).

[7] Z. Chai, Ph.D. thesis, Massachusetts Institute of Technology, 2003.

[8] R. E. Roché, Ph.D. thesis, Florida State University, 2003.

[9] K. Joo *et al.*, Phys. Rev. Lett. **88**, 122001 (2002).

[10] D. Drechsel, O. Hanstein, S. S. Kamalov, L. Tiator, and S. N. Yang, www.kph.uni-mainz.de/MAID.

[11] D. Drechsel, O. Hanstein, S. S. Kamalov, L. Tiator, and S. N. Yang, www.kph.uni-mainz.de/MAID/dmt/dmt2001.html.

[12] R. A. Arndt, W. J. Briscoe, R. L. Workman, and I. I. Strakovsky, gwdac.phys.gwu.edu.